Available online at www.sciencedirect.com

SciVerse ScienceDirect

Journal of the European Ceramic Society 32 (2012) 2073–2085

www.elsevier.com/locate/jeurceramsoc

Probabilistic lifetime prediction for ceramic components in rolling applications

M. Härtelt *,[1], H. Riesch-Oppermann, I. Khader, O. Kraft

Institute for Applied Materials, Karlsruhe Institute of Technology (KIT), Karlsruhe, Germany

Received 12 August 2011; received in revised form 16 December 2011; accepted 7 January 2012
Available online 14 February 2012

Abstract

Rolling tools made of advanced ceramics have some attractive properties with respect to their wear resistance and high temperature performance but are critical due to the brittle failure mode. Lifetime predictions must be based on a probabilistic approach considering sub-critical and cyclic propagation of the inherent flaws. We will present a comprehensive reliability analysis for a rolling contact fatigue test with a silicon nitride roll using the program STAU. Based on a cyclic crack growth law, we have extended the capabilities of STAU in order to account for a complex load history typically found in the case of rolling applications. A scheme is presented for relating the failure probability to the crack density observed on the roll which allows for a quantitative comparison of predictions and experimental observations. It turns out that the water-based lubrication most critically affects the failure behaviour since water strongly promotes cyclic crack propagation.

Keywords: Failure analysis; Fatigue; Lifetime; Si_3N_4; Weibull statistics

1. Introduction

Advanced ceramics are promising materials for applications operating at high temperature and/or severe tribological conditions. Silicon nitride (Si_3N_4) is a preferred material for metalworking tools due to its outstanding wear resistance and high strength at elevated temperatures. One of the main challenges in designing reliable components for such applications is the brittle fracture behaviour of ceramics, which has been in the focus of recent research on silicon nitride rolling tools. Lengauer and Danzer[1,2] conducted a comprehensive fracture mechanics study on the failure of industrial Si_3N_4 rolls. They showed that the initiation of large cracks on the roll calibre is controlled by tensile stresses when processing superalloy wires. Lab-scale rolling tests (Khader and Kailer[3]) using high strength steel wires showed that there is a time-dependent evolution of cracks on the calibre surface. However, the role of natural flaws (such as grinding cracks) on the failure of ceramic rolling tools has not yet been studied extensively. One crucial task is to investigate how crack propagation caused by repeated cyclic loading can influence the initiation of large cracks and damage on the rolls.

Predicting the failure of ceramic components must be based on probabilistic methods in order to cope with the large scatter in crack size which is characteristic for the inherent flaw population. Fracture occurs once the most unfavourable natural flaw in terms of location and orientation exceeds a critical size and initiates unstable crack propagation. Consequently, the scatter in flaw size results in scatter in strength and lifetime as well as in a size effect. The stochastic nature of the inherent flaws can be accounted for using the mathematical framework of the Weibull theory[4] based on a weakest-link model. Numerical tools such as STAU[5] or the CARES code[6] have been established as post-processors for a finite element (FE) stress analysis for failure predictions of components under complex transient loading. Time-dependent failure of ceramics is caused by slow propagation of natural cracks in the material. Under (quasi-)static loading, crack propagation is promoted by sub-critical crack growth which is strongly affected by environmental conditions.[7] For toughened ceramics, e.g. by grain-bridging,

* Corresponding author at: Bombardier Transportation GmbH, Holländische Strasse 195, 34127 Kassel, Germany. Tel.: +49 561 801 5277, fax: +49 561 801 6701.
E-mail address: martin.haertelt@de.transport.bombardier.com (M. Härtelt).
[1] Based in part on the dissertation by M. Härtelt at the Karlsruhe Institute of Technology, KIT, 2010.

0955-2219/$ – see front matter © 2012 Elsevier Ltd. All rights reserved.
doi:10.1016/j.jeurceramsoc.2012.01.009

crack propagation is enhanced under cyclic loading due to the relative movement of interlocked crack faces that shield the crack tip.[8] Cyclic wear degradation of the bridging elements leads to progressive increase of the effective stress intensity factor which may assist further sub-critical crack growth. Both sub-critical and cyclic crack growth can be described by empirical power laws which are easy to integrate into the mathematical framework of a probabilistic failure analysis.

The effect of sub-critical crack growth on component lifetime has been studied by Brückner-Foit and Ziegler[9] for a SiC fastening bolt in a gas turbine casing using the STAU program. A study on Si_3N_4 engine valves by Nemeth et al.[6] based on a combined approach for sub-critical and cyclic crack growth showed that lifetime predictions differ by many orders in magnitude depending on which underlying fatigue mechanism is assumed. However, careful comparisons of probabilistic lifetime predictions with experimental observations for components that have actually failed have rarely been described in literature.

In this paper we will present a comprehensive probabilistic reliability analysis using the example of a rolling contact fatigue (RCF) test with a commercial silicon nitride grade (SL200). For that purpose, we will extend the lifetime prediction procedures used in STAU by an approach for cyclic crack propagation. Special attention is paid to obtaining the necessary information about the cyclic load history which is required for the analysis. Damage in the RCF experiment is characterized by time-dependent initiation of macroscopic cracks on the roll surface. This allows for evaluating the prediction results in conjunction with the time-dependent evolution of the crack density. Results presented here are based on parameters from sub-critical and cyclic crack propagation in air and water, as they exhibit strong differences in the calculated lifetimes and failure probabilities. We will show that the observed crack density can be predicted if uncertainties in the fatigue parameters of the considered material silicon nitride SL200 are taken properly into account.

2. Theory

Failure of ceramics is characterized by inherent natural or processing flaws which can be treated as cracks. A component fails as soon as the most unfavourable natural crack exceeds a critical size, a_c, which depends on the location, orientation of the crack and on the fracture toughness of the material. A failure criterion can be formulated based on a local fracture mechanics approach ('Batdorf'-model[10]) in which the (critical) flaw size a (a_c) is replaced by a (critical) Mode-I equivalent stress $\sigma_{eq}(\vec{r}, \Omega)$ depending on the location $\vec{r}$ and orientation Ω of the crack[a]:

$$K_{Ieq} = \sigma_{eq} Y_I \sqrt{a} \leftrightarrow K_{Ic} = \sigma_{eq} Y_I \sqrt{a_c} \tag{1}$$

Failure occurs if the equivalent stress intensity factor K_{Ieq} exceeds the fracture toughness of the material K_{Ic}. The geometry factor Y_I refers to the respective fracture mechanics model for natural flaws. The equivalent stress is determined by an appropriate mixed-mode criterion, for example the widely used 'normal stress' criterion which considers pure Mode-I contributions only.[11]

2.1. Failure probability under cyclic fatigue

The time-dependent propagation of natural flaws must be considered for materials which exhibit cyclic crack growth. A detailed description of the way how (sub-critical) crack propagation is treated in a probabilistic analysis of engineering structures can be found in Brückner-Foit and Ziegler.[9] Adopting this procedure, a formulation for failure under fatigue can be found by integrating a cyclic crack propagation law (see also Nemeth et al.[6]). An overview on crack growth laws applicable for ceramics can be found in Fett and Munz.[12] Crack propagation is most commonly described by a power-law which relates the crack growth rate da/dN with the applied stress intensity factor range $\Delta K = K_{max} - K_{min}$ normalized by the fracture toughness K_{Ic}:

$$\frac{da}{dN} = A\left(\frac{\Delta K_I}{K_{Ic}}\right)^n. \tag{2}$$

The parameters n and A are material properties. The crack propagation rate da/dN may also depend on the load ratio $R = K_{min}/K_{max}$. Assuming that n is independent of R, the influence of the load ratio can be expressed using a second exponent p and a corresponding parameter C different from A:[13]

$$\frac{da}{dN} = \frac{C}{(1-R)^{n-p}}\left(\frac{\Delta K_I}{K_{Ic}}\right)^n. \tag{3}$$

Under transient loading, the critical crack size a_c is also time-dependent as illustrated in Fig. 1(a). The time t_f at which spontaneous failure occurs is determined by the minimum $a_{c,min}$ within the considered time interval. In the case of slow crack propagation (sub-critical/cyclic), there is a corresponding critical initial crack size $a_{c,0}$ which is relevant for evaluating the reliability based on defect statistics. In the case of cyclic loading, the load history can be expressed in terms of the equivalent stress $\sigma_{eq}(t)$ as shown in Fig. 1(b). Each load cycle is characterized by an individual stress range $\Delta\sigma_{eq}(N) = \sigma_{eq,max}(N) - \sigma_{eq,min}(N)$ and a corresponding load ratio $R(N) = \sigma_{eq,min}(N)/\sigma_{eq,max}(N)$. Based on Eq. (1), ΔK_I^n can be formulated in terms of the crack length a and $\Delta\sigma_{eq}$:

$$\begin{aligned}\Delta K_I^n(N) &= Y_I^n(\Delta\sigma_{eq}(N))^n a^{n/2} \\ &= Y_I^n[\sigma_{eq,max}(N)(1-R(N))]^n a^{n/2}.\end{aligned} \tag{4}$$

Introducing Eq. (4) in Eq. (3), the critical initial crack size can be determined by integrating the crack growth relation

$$\begin{aligned}\frac{da}{dN} &= \frac{C\cdot Y_I^n}{K_{Ic}^n}\cdot(\sigma_{eq,max}(N))^n\cdot(1-R(N))^p\cdot a^{n/2} \\ &\rightarrow \int_{a_0}^{a_i} a^{-n/2}\,da = \frac{C\cdot Y_I^n}{K_{Ic}^n}\int_0^{N_i}(\sigma_{eq,max}(N))^n\cdot \\ &(1-R(N))^p\,dN\end{aligned} \tag{5}$$

[a] The dependence of σ_{eq} on $\vec{r}$ and Ω will not be denoted explicitly in the following derivations.

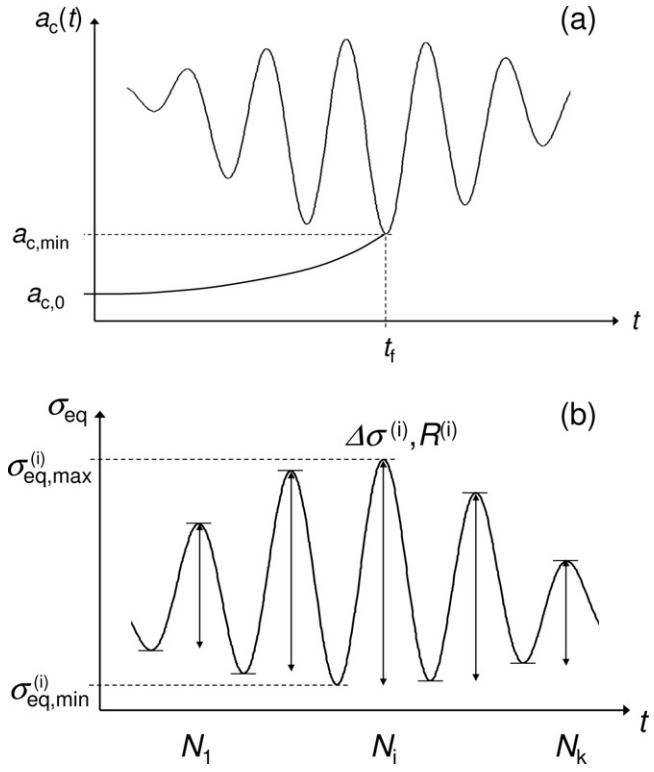

Fig. 1. (a) Critical crack size a_c and initial critical crack size $a_{c,0}$ under time-dependent (cyclic) loading; (b) time-dependent sequence of the equivalent stress σ_{eq} for a load history of N_k individual cycles.

which yields (for $n \neq 2$):

$$a_0 = \left[a_i^{(2-n)/2} + \frac{(n-2)\cdot CY_I^n}{2K_{Ic}^n} \int_0^{N_i} \left(\sigma_{eq,max}(N)\right)^n \cdot (1-R(N))^p \, dN \right]^{2/(2-n)}. \tag{6}$$

Eq. (6) provides a relation between the initial crack size a_0 and the crack size a_i after N_i cycles. If the component fails after N_i cycles, a_i can be replaced by a_c (Eq. (1)) and the critical initial crack size reads:

$$a_{c,0} = \left[\left(\frac{K_{Ic}}{\sigma_{eq,max}(N_i)} \right)^{2-n} + \frac{(n-2)\cdot C \cdot Y_I^n}{2K_{Ic}^n} \times \int_0^{N_i} (\sigma_{eq,max}(N))^n \cdot (1-R(N))^p \, dN \right]^{2/(2-n)}. \tag{7}$$

The probability F that $a_{c,0}$ is exceeded can be determined assuming a flaw size distribution of the type $f_a \approx a^{-r}$:

$$F(a \geq a_{c,0}) = \left(\frac{\tilde{a}}{\min\limits_{N \in [0,N_k]} \left[a_{c,0}(N)\right]} \right)^{r-1} \tag{8}$$

$\tilde{a}$ is a threshold crack size below which failure is not expected. It is important to note that Eq. (8) must be evaluated for the minimum value of $a_{c,0}$ which depends on the considered cycle N within the interval $[0,N_k]$.

Predicting the failure probability of a component under complex loading requires to consider an arbitrary number of randomly orientated and located cracks. For cyclic fatigue, the probability of the whole component is given by Eq. (9), a detailed derivation can be found in Appendix A:

$$P_f = 1 - \exp\left(-\frac{1}{V_0} \int_V \frac{1}{4\pi} \int_\Omega I \, d\Omega \, dV \right)$$
$$I = \max_{\eta \in [0,N_k]} \left[\left(\frac{\sigma_{eq,max}(\eta)}{\sigma_0} \right)^{n-2} + \frac{\sigma_0^2}{B} \int_0^\eta \left(\frac{\sigma_{eq,max}(N)}{\sigma_0} \right)^n \cdot (1-R(N))^p \, dN \right]^{\frac{m}{n-2}} \tag{9}$$

The failure probability is calculated by an integral over the component volume[b] V and crack orientation Ω. V_0 is a unit volume. The integral must be solved over 5 dimensions: three spatial coordinates (V) and two crack orientation coordinates (Ω). The integrand, I, is composed of two parts: The first term refers to spontaneous failure, the second term represents the contribution by cyclic crack propagation via an integral over the individual cyclic load history. The integration over the component volume and crack orientation is performed using the maximum value of I at each cycle within the considered interval of N_k cycles. The material specific parameters m (Weibull modulus) and σ_0 (normalized strength with respect to V_0) are associated with the strength of the material and can be derived from inert strength tests; η is a dummy variable for cycle numbers. The fatigue behaviour is characterized by the parameters n, p and B, in which B refers to the crack growth parameter C and is calculated by Eq. (10):

$$B = \frac{2K_{Ic}^2}{CY_I^2(n-2)} \tag{10}$$

A similar formulation as Eq. (9) is obtained when integrating the power-law for sub-critical crack growth (Appendix C).[9]

Evaluating Eq. (9) can become computationally expensive if the cyclic load history is repeated in a periodical manner such as in the case of a stationary rolling process. Assuming that the load history is repeated Z times, the cycle-dependent term in the integrand I of Eq. (9) can be reformulated using the contribution of the first full $(Z-1)$ repetitions as shown in Eq. (11):

$$I = \max_{\eta \in [0,N_k]} \left[\left(\frac{\sigma_{eq,max}(\eta)}{\sigma_0} \right)^{n-2} + \frac{\sigma_0^2}{B} \left(\int_0^\eta \left(\frac{\sigma_{eq,max}(N)}{\sigma_0} \right)^n \cdot (1-R(N))^p \, dN \right) + (Z-1) \cdot \frac{\sigma_0^2}{B} \left(\int_0^{N_k} \left(\frac{\sigma_{eq,max}(N)}{\sigma_0} \right)^n \cdot (1-R(N))^p \, dN \right) \right]^{\frac{m}{n-2}} \tag{11}$$

Here, the failure probability is determined only by the number of repetitions Z. For a high Z, the 'cyclic' term becomes pre-

[b] The corresponding formula for a surface flaw model can be found in Appendix B.

dominant compared to the 'static' contribution. In this case, the term for spontaneous failure can be neglected and finding the maximum of I becomes obsolete. As a consequence, the integrand can be simplified in such a way that P_f can be expressed in terms of a Weibull distribution with the Weibull parameters m^* and N_0:

$$P_f(Z) = 1 - \exp\left[-\left(\frac{Z}{N_0}\right)^{m^*}\right]$$
$$m^* = \frac{m}{n-2} \tag{12}$$
$$N_0 = \left[\frac{1}{V_0}\int_V \frac{1}{4\pi}\int_\Omega \left(\frac{\sigma_0^2}{B}\int_0^{N_k}\left(\frac{\sigma_{eq,max}(N)}{\sigma_0}\right)^n \cdot (1-R(N))^p \, dN\right)^{m/(n-2)} d\Omega \, dV\right]^{-1/m^*}$$

N_0 is the 63%-quantile of the lifetime distribution and will henceforth be denoted as 'characteristic lifetime'.

2.2. Numerical implementation

Solving the integrals in Eqs. (9), (11) and (12) requires numerical integration procedures based on a FE stress analysis of the un-cracked component. The post-processor STAU is a numerical tool that employs a Gauss-quadrature scheme based on the element stresses provided with the FE results. Sufficient accuracy is achieved by generating a number of additional evaluation points within the numerical integration procedure using the interpolation functions of the FE formulation. A detailed description of STAU can be found in Riesch-Oppermann et al.[5]

If sub-critical crack growth is considered in the analysis (Appendix C, Eq. (C.2)), an integral over the complete load history $\sigma_{eq}(t)$ must be solved for each evaluation point $(\vec{r}, \Omega)$ of the integration. In the case of cyclic fatigue, only the contribution of the individual cycles is taken into account. Consequently, the maximum and minimum values of the equivalent stress must be identified for any evaluation point within the calculation run. For that purpose, the maximum principal stress σ_1 is tracked for every spatial evaluation point in order to reduce the numerical effort. The peaks of σ_1 coincide with the peaks of σ_{eq} if the normal stress criterion is used as mixed-mode criterion to determine the equivalent stress. Once the time increments which refer to the minima and maxima of σ_{eq} are identified for each individual cycle, the integrand I can be calculated for a corresponding set of $\sigma_{eq,max}$ and R. Due to the discrete nature of cyclic crack growth, the integral over the cyclic load history can be replaced by a sum over all cycles:

$$\int_{N_1}^{N_k}\left(\frac{\sigma_{eq,max}(N)}{\sigma_0}\right)^n (1-R(N))^p \, dN = \sum_{i=1}^{k}\left(\frac{\sigma_{eq,max}(N_i)}{\sigma_0}\right)^n (1-R(N_i))^p \tag{13}$$

3. Material properties of silicon nitride SL200

SL200 (Ceramtec, Germany) is a commercial silicon nitride quality with 3 wt.% Al_2O_3 and 3 wt.% Y_2O_3. The strength distribution was determined in standard[14] 4-point-bending tests with a specimen size of 45 mm × 4 mm × 3 mm and a sample size of 24.[15,18] The Weibull parameters are shown in Table 1(a). The mechanical properties and sub-critical crack growth (SCG) behaviour of SL200 was also investigated in a comprehensive study by Lube and Dusza[16] for different temperatures. They report a lower value for the 4-point-bending strength which might be due to a different sintering route or surface finishing process. The required SCG parameters in ambient air were adopted from their work and are summarized in Table 1(b).

The fatigue behaviour in ambient air was determined for the two load ratios $R = 0.1$ and $R = 0.5$ by cyclic tests under different load levels at a frequency of 60 Hz.[15] Crack propagation curves for natural flaws can be calculated by an indirect method combining strength and lifetime tests.[17] Lifetimes were pooled in order to decrease uncertainties in the crack growth curves associated with the sparse underlying database obtained for each load level.[18] The curves are presented in Fig. 2(a). Crack growth parameters were determined by fitting the curves with Eqs. (2) and (3), the corresponding parameters can be found in Table 2(a). In principle, the 3-parameter crack propagation law Eq. (3) does not account for a variation in n. On the other hand, different crack growth exponents are obtained for different load ratios when evaluating using Eq. (2).[18] The straight lines in Fig. 2(a) show how both empirical laws represent the crack growth curves. It turns out that corresponding parameters of the extended law Eq. (3) can adequately render the data except for the rightmost part of the curve measured at $R = 0.5$.

Table 1
Material parameters of Si_3N_4-SL200: (a) Weibull parameters m and σ_{4PB} from 4-point-bending strength tests, numbers in braces indicate 90% confidence level; (b) sub-critical crack growth parameters n_{sub}, A_{sub} from 16; B_{sub} is calculated by Eq. (10) using $K_{Ic} = 4.9$ MPa m$^{0.5}$ [16] and $Y_I = 1.3$ (recommended for semi-circular flaws[17]).

	m		σ_{4PB} [MPa]
(a) Strength	11.5 (8.7;15.1)		1044 (1012;1077)
	n_{sub}	A_{sub} [m/s]	B_{sub} [MPa^2 s]
(b) Sub-critical crack growth[16]	42	10^{-6}	7.1×10^5

Table 2
Cyclic crack growth parameters of Si_3N_4-SL200 for (a) 2-parameter law and (b) 3-parameter law for air and water. B follows from Eq. (10) using $K_{Ic} = 5.65$ MPa $m^{0.5}$ [18] and $Y_I = 1.3$.

Medium	R	(a) 2-Parameter law (Eq. (2))		(b) 3-Parameter law (Eq. (3))			
		n	A [m/cycle]	n	p	C [m/cycle]	B [MPa^2 cycle]
Air[18]	0.1	20.1	5.8×10^{-8}	24.4	2.2	2.8×10^{-8}	6.1×10^{7}
	0.5	30.8	5.6×10^{1}				
Water	0.5	29.9	1.1×10^{4}	29.9	2.2	4.9×10^{-5}	2.7×10^{4}

In addition to the cyclic tests in air, lifetimes were measured in distilled water at $R = 0.5$.[19] The crack growth curve was calculated using the same pooling strategy[18] as for the curves in air. The crack growth curve for water is shown in Fig. 2(b) along with the corresponding curve in air. The crack propagation rate is increased by about two orders in magnitude under water. The corresponding crack growth parameters are given in Table 2(b). It should be noted that the exponent n remains almost unaffected if compared to the results in air at $R = 0.5$. It is not straightforward to determine the crack growth parameters of Eq. (3) since only one load ratio was tested in water. Therefore, we assume that the exponent p remains unaffected under water which allows for calculating C from A by combining Eqs. (2) and (3):

$$C = A(1 - R)^{n-p} \tag{14}$$

The parameters are summarized in Table 2(b).

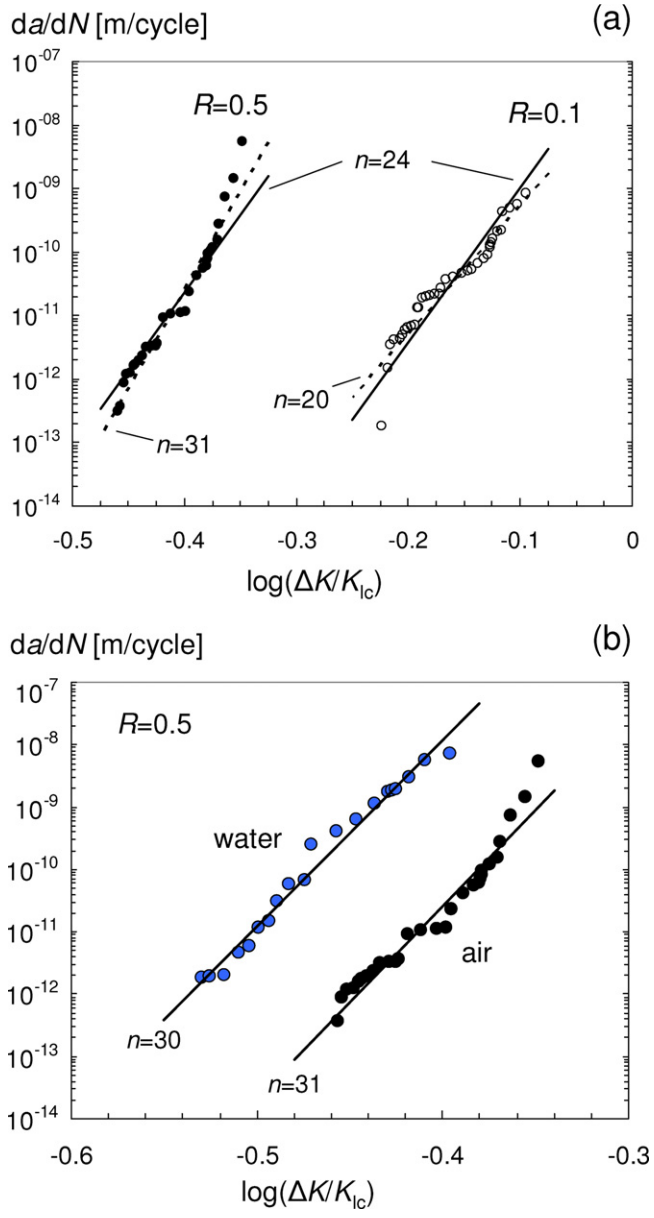

Fig. 2. Cyclic crack growth curves calculated from cyclic tests in (a) air for $R = 0.1/0.5$[18] and (b) in air and water for $R = 0.5$.

4. Results

4.1. Rolling contact fatigue test

The rolling contact fatigue tests considered in the present work were conducted by Khader[20] in order to study the mechanical and tribological damage mechanisms of ceramic rolls under different conditions. The test principle is shown in Fig. 3, and the relevant parameters are summarized in Table 3. Hardened 100Cr6 steel discs (HV10 > 800) with a circular curved profile (radius 5 mm) are brought in contact with a cylindrical silicon nitride SL200 roll. The applied normal force $F_A = 1700$ N leads to a maximum contact pressure of about ~4.55 GPa. A constant slip of ~22% is realized by the difference in rotational speed ω_1/ω_2 of the rolls. The experiment was run using an emulsion of 5% oil-based lubricant (UNOPOL G 600) in de-ionized water. A friction coefficient of $\mu = 0.085$ was measured during the tests.

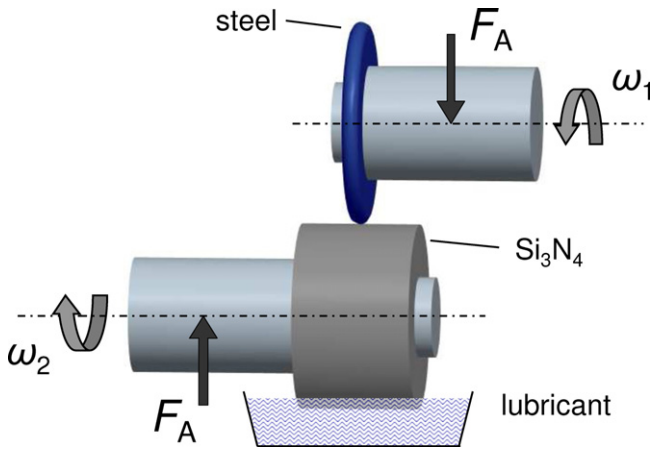

Fig. 3. Schematic view of the rolling contact fatigue (RCF) test setup. F_A – normal force; ω_1/ω_2 – rotary speed of the rolls (for details see Table 3).

Table 3
Rolling contact fatigue (RCF) test parameters and elastic material properties.

Material	Elastic properties	Diameter	Rotary speed	Contact force F_A	Friction coefficient
100Cr6	$E = 210$ GPa, $\upsilon = 0.3$	60 mm	$\omega_1 = 200\,\text{min}^{-1}$	1700 N	0.085
Si_3N_4-SL200	$E = 300$ GPa, $\upsilon = 0.29$	55 mm	$\omega_2 = 175\,\text{min}^{-1}$		

The maximum duration of the tests was 15 h. Damage on the roll surface was analysed after different test periods by examining light microscopy and SEM images of the corresponding wear tracks. Isolated cracks can be observed immediately after a few rotations. After 10 h (or 105,000 rotations), a dense network of cracks is visible on the surface of the roll (Fig. 4(a)). After 15 h (Fig. 4(b)), the number of cracks has increased whilst existing cracks seem to propagate further along the surface. It is difficult to provide an exact crack density value, since crack bifurcation and secondary crack initiation is observed. Therefore, we decided to estimate the crack density estimate based on the principal features of the observed pattern of curved cracks which is demonstrated for the crack pattern after 10 h in Fig. 4(a). In this case, we obtain a crack density of about 4–5 cracks per mm.

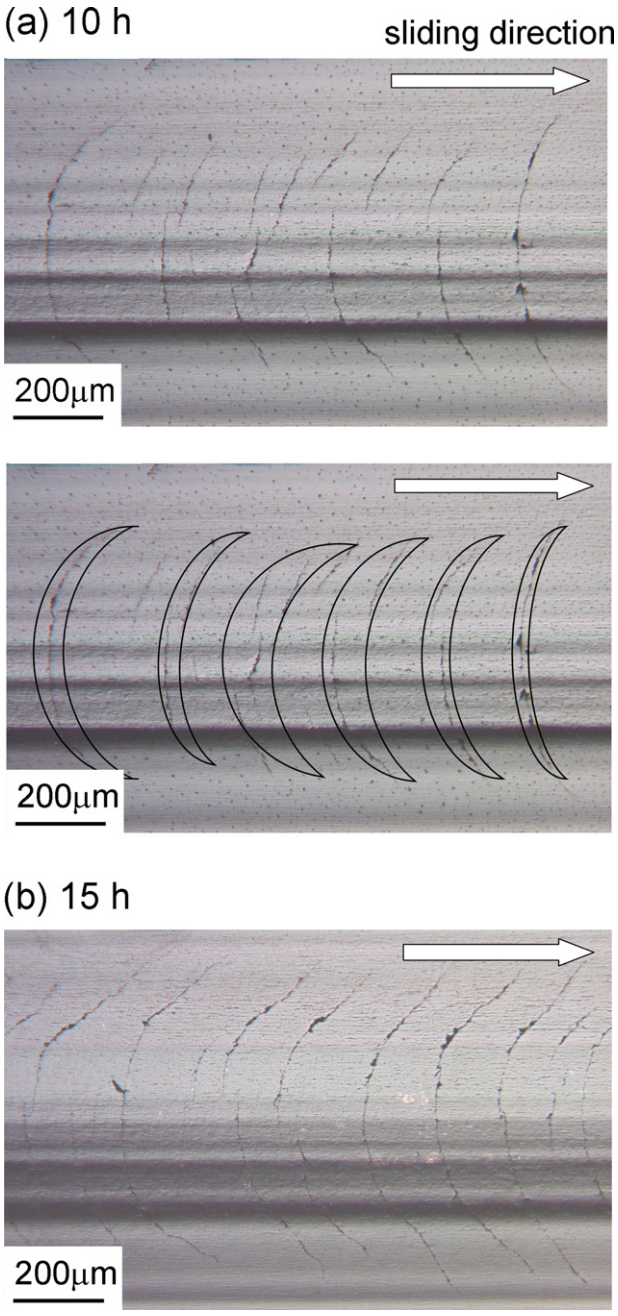

Fig. 4. Crack network on the surface of the Si_3N_4-disc after a test period of (a) 10 h and (b) 15 h. The main crack features used for estimating the crack density after 10 h are indicated.

The macroscopic cracks have a partial cone crack shape which is typical for brittle materials under sliding loads.[21] The cross-sectional view of the roll in Fig. 5 shows the path of a partial cone crack which kinks under the surface. The first principal stress trajectories obtained by the finite element stress analysis are superimposed to the picture. In the early stage, the crack path is nearly perpendicular to the surface. Crack kinking starts approximately 10 µm below the surface under the influence of Mode-II contributions.

4.2. Finite element simulation

The stress distribution of the roll was determined by a finite element analysis using ABAQUS/Standard. The ceramic and the steel disc were modelled as isotropic elastic materials using the elastic properties given in Table 3. Resolving the peaks of the

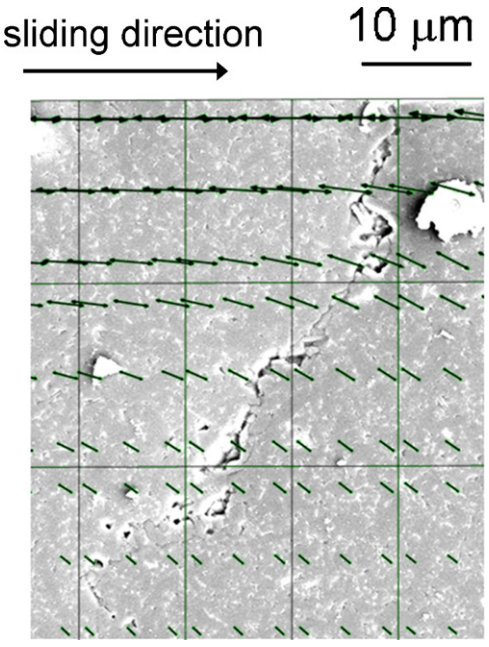

Fig. 5. Cross-sectional view of a partial cone crack superimposed to the first principal stress trajectories from FE-analysis.

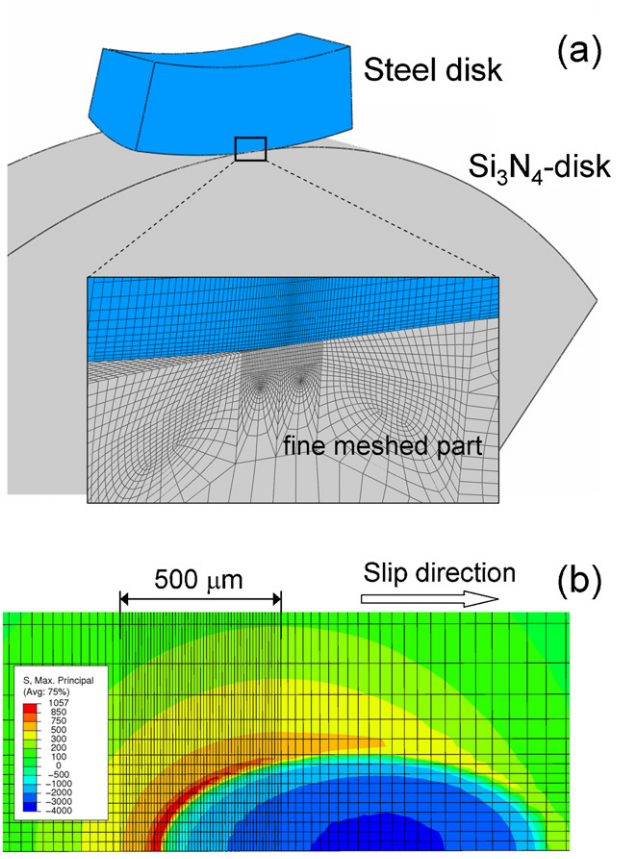

Fig. 6. (a) Cross-section view of the finite element model with the fine-meshed part; (b) distribution of the maximum principal stress on the roll groove of the Si_3N_4 disc surface.

tensile stresses in the wake of the contact zone requires a highly refined meshing of the region under consideration. Moreover, the time increments of the finite element analysis must be chosen such that peaks of the stress history are resolved for each element of the fine-meshed region. Therefore, the analysis is only possible for a relatively small section of the roll containing a region with a highly refined mesh, which is considered in the subsequent STAU calculation. The modelled section is shown in Fig. 6(a). The symmetry plane in the centre of the contact zone is also accounted for by the model.

The fine meshed part of the ceramic roll extends over a length of 500 µm along the circumferential direction as can be seen in Fig. 6(b). The mesh consists of 20-node quadratic brick elements which allow for an accurate reproduction of the tensile peak stresses. The analysis is conducted in several subsequent steps. First, contact is established outside the refined mesh region and the rolls are rotated until the contact zone approaches the refined mesh boundary. As the wake of the contact zone passes through the finely meshed region, time increments are refined to adequately render the stress history. Fig. 6(b) shows the distribution of the maximum principal stresses on the surface of the Si_3N_4 roll in the fine meshed region. Tensile stresses are maximal in the symmetry plane giving peak stress values of about 1100 MPa. The characteristic shape of partial cone cracks (Fig. 4) is in agreement with the first principal stress distribution on the surface. The crack path under the surface coincides

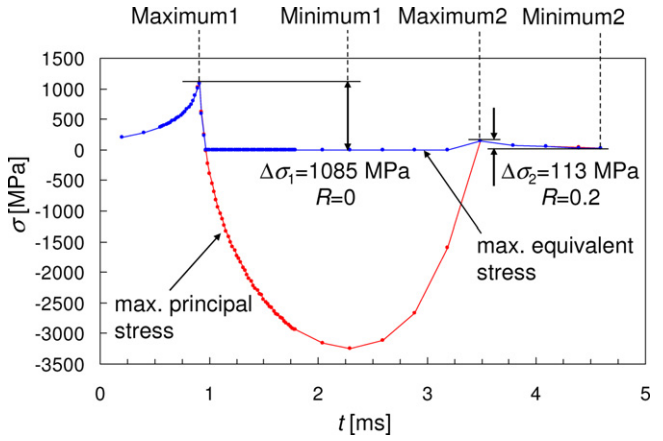

Fig. 7. Stress history at the centre position on the roll groove: cycles are determined from the max./min. principal stress peaks, equivalent stress is calculated by STAU (normal stress criterion).

with the trajectories of the first principal stress showing that the crack propagated normal to the maximum tensile stress (Fig. 5).

4.3. Prediction of lifetime and crack density

4.3.1. General approach

For the lifetime prediction under cyclic crack growth it is necessary to determine the individual cyclic load history for each spatial evaluation point using the time sequence of the first principal stress. A typical load history can be seen in Fig. 7, for which the corresponding evaluation point is located in the middle of the roll calibre where tensile stresses are at their maximum value. The figure shows the first principal stress history and the maximum equivalent stress σ_{eq} obtained by STAU for this point at the most unfavourable orientation. σ_{eq} is calculated by the normal stress criterion which is adequate to describe the failure behaviour of micro-cracks in silicon nitride.[11] The peaks of the first principal stress match the peaks of the equivalent stress exactly except for the section governed by compressive stresses where cracks are expected to be closed and therefore $\sigma_{eq} = 0$. During the load history shown in Fig. 7, two stress cycles can be identified with stress ranges of $\Delta\sigma_1 = 1085$ MPa and $\Delta\sigma_2 = 115$ MPa. The first cycle corresponds to the maximum and minimum #1 with the tensile zone ahead of the contact area. The load ratio is $R = 0$ due to the following compression zone. The second peak occurs after passing the contact zone with a weaker tensile stress.

The contact damage observed in the experiments consists of a number of macroscopic cracks which are supposed to be originated from natural surface defects. This raises the question how to relate the failure probability calculated by STAU with the observed crack density. In principle, P_f describes the probability that one crack in the considered section becomes critical and causes a macroscopic crack. Adopting this argument to the RCF test implies that we predict the probability of having one observable crack, seen as a partial cone crack, in the modelled section of the roll after a given number of rotations. The crack density, for which we calculate P_f, is given by the size of the

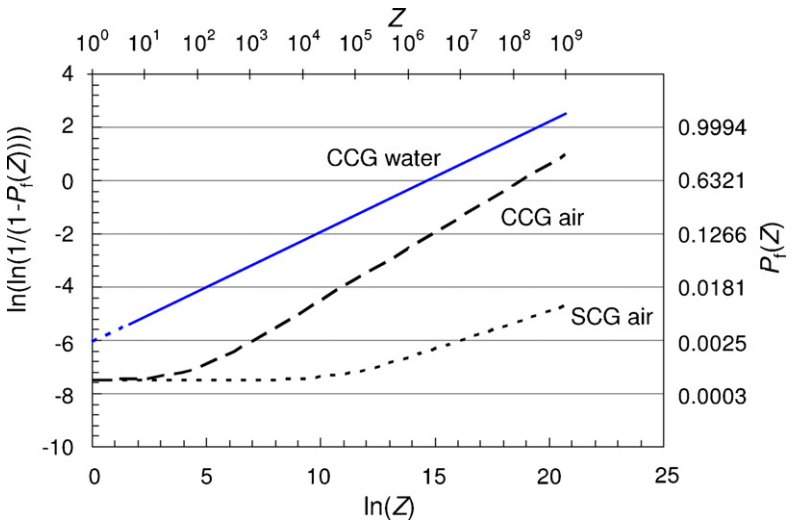

Fig. 8. Probability to initiate 4 cracks per mm along the roll circumference depending on the number of rotations Z. Different fatigue parameters were used: Sub-critical (SCG) and cyclic crack growth (CCG) in air; CCG in water (Tables 1 and 2(b)).

roll section considered in STAU and its relation to the full roll circumference. Therefore, it is useful to define the crack density Φ as number of cracks along the circumferential direction normalized by a unit length, e.g., number of cracks per mm. As we calculate the failure probability for the fine-meshed section of 500 μm (Fig. 6(b)), this corresponds in principle to one crack every 500 μm ($\Phi = 2\,\mathrm{mm}^{-1}$). However, since a half symmetric FE model was used for the roll, the failure probability actually corresponds to a crack density of $\Phi = 4\,\mathrm{mm}^{-1}$ which accounts for the fact that only half the volume or surface is considered in the STAU subsequent analysis.[c]

4.3.2. Lifetime distributions

First, results will be presented for the specific crack density $\Phi = 4\,\mathrm{mm}^{-1}$, which is also typically seen in the experiments after 10 h of rolling (Fig. 4(a)). Sub-critical crack growth (SCG) and cyclic crack growth (CCG) were each considered in separate analysis runs. In order to account for the different fatigue parameters available in the case of CCG, it is further distinguished between parameters measured in air and water (Table 2(b)).

The failure probability was calculated based on the fracture mechanics model of surface flaws using the normal stress criterion as mixed-mode criterion. The normalized strength parameter σ_0 is calculated automatically in STAU from the 4-point bending strength (Table 1(a)) based on the normal stress criterion. This calculation requires the geometry of the 4-point-bending specimen as well as the Weibull modulus. For a surface flaw analysis, we obtain $\sigma_0 = 1321$ MPa which refers to a unit area of $A_0 = 1\,\mathrm{mm}^2$. The following STAU predictions refer to this specific choice of the unit area.

The results are presented in Fig. 8 in terms of a Weibull diagram for the different fatigue conditions considered. The slope of the curves represents the Weibull parameter m^* of the lifetime distribution as given in Eq. (12).

The curves obtained for SCG and CCG (Fig. 8) show that the failure probability is strongly affected by the fatigue parameters corresponding to the different environmental conditions which were considered. The damaging effect of cyclic fatigue becomes obvious by comparing the SCG/CCG curves in air. Whilst the CCG failure probability starts to increase after about a few rotations, the SCG curve remains at the level of spontaneous failure probability for almost 10^4 rotations. The difference between the two curves is further enhanced by the difference in n which is reflected by the slopes. The failure probability in the case of CCG is further increased if fatigue parameters under water are considered. Here, the 'cyclic' term (Eq. (11)) becomes predominant from the very beginning which can be seen from the fact that the failure probability increases from the first load cycle.

The considered crack density $\Phi = 4\,\mathrm{mm}^{-1}$ in the analysis can be used to assess the quality of the predictions with respect to the crack density found after 10 h in the RCF test (Fig. 4(a)). The failure probability after 10 h (105,000 rotations) and the characteristic lifetimes from Eq. (12) are summarized in Table 4. It turns out that only predictions for cyclic crack growth based on fatigue parameters in water can roughly meet the experimental results. However, the predicted 63%-quantile in lifetime (N_0) indicates, that the observed crack density is actually not likely to be expected within a test duration of $N_0 = 2.4 \times 10^6$ rotations (≈230 h).

It was shown above that the crack growth exponent n obtained from measurements in air depends on the load ratio R (Table 2(a)). From the experimental data in water, n is only known for one specific value $R = 0.5$. Assuming a similar behaviour as in air (n decreases with decreasing R) under water ambience, the n-values for a smaller R can be expected to be lower. Therefore, the influence of n is addressed in a parametric study conducted using a range of $n = 20$–30. According to Eq. (10), B must be re-calculated (see Table 5(a)) for different values of n based on the crack growth parameter A obtained for water. The failure probability and the corresponding N_0 results are presented in Fig. 9(a). It is seen that the characteristic

[c] See also Appendix D.

Table 4
Probability of crack initiation (crack density $\Phi = 4\,mm^{-1}$) section calculated for different failure mechanisms after a test period of 10 h.

Failure mode	Spontaneous rupture	Sub-critical crack growth (air)	Cyclic crack growth (air)	Cyclic crack growth (water)
P_f ($Z = 105{,}000$)	5.5×10^{-4}	7.5×10^{-4}	2.4×10^{-2}	0.24
N_0	–	–	1.5×10^{8}	2.4×10^{6}

Table 5
Crack growth parameter B calculated for a variable exponent: (a) n ($p = 2.2$) and (b) p ($n = 29.9$) via Eqs. (10) and (14) based on A obtained for water at $R = 0.5$ (Table 2(a)) using the fracture mechanics parameters $K_{Ic} = 5.65\,MPa\,m^{0.5}$ [18] and $Y_I = 1.3$.

(a)	n					
	20	22	24	26	28	30
B [MPa^2 cycle]	4.3×10^4	3.8×10^4	3.5×10^4	3.2×10^4	2.9×10^4	2.7×10^4

(b)	p				
	0	1	2	3	4
B [MPa^2 cycle]	1.2×10^5	6.2×10^4	3.1×10^4	1.6×10^4	7.8×10^3

lifetime drops below 10 h for n-values less than 25. In the case of $n \approx 20$, the probability for initiating the observed crack density increases to about 100%. A second parametric study assesses the influence of the exponent p, which was adopted from measurements in air to allow for using the 3-parameter law (Eq. (3)) in the case of water. Besides the fact that p has an impact on the numerical integration, it also affects the parameter C calculated by Eq. (14). As a consequence, B depends on p as given in Table 5(b). Despite the strong impact of p on B, the variation of the failure probability and the characteristic lifetime is moderate compared with the influence of n as can be seen in Fig. 9(b).

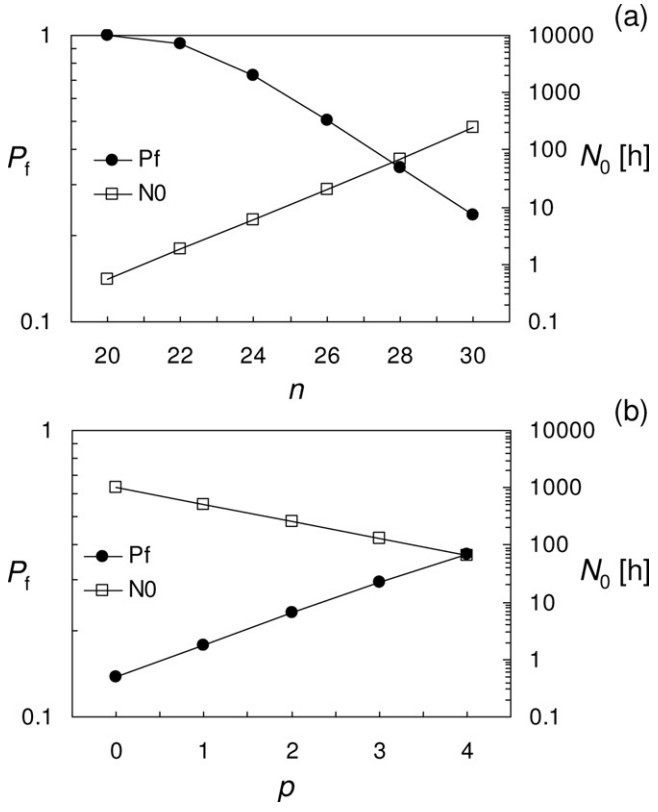

Fig. 9. Parametric study on the influence of the exponents (a) n ($p = 2.2$) and (b) p ($n = 29.9$) on the crack initiation probability (4 cracks per mm) and the corresponding characteristic lifetime N_0.

4.3.3. Crack density

The previous analysis has focused on the probability of initiating a specific crack density on the roll surface. The damage on the roll can also be addressed by calculating the expected crack density after a given number of rotations. In this case, the size of the roll section considered in STAU is modified in a way that the section size corresponds to just the mean distance of the cracks with given density. This can be done by defining a multiple of the integrand (Eqs. (9)–(12)) which acts as a scaling factor within the STAU analysis. For this approach to be valid, we rely on the assumption that the modelled section on the roll (with a length of 500 μm) sufficiently represents the transient loads in a stationary process. A detailed derivation of the relation between the crack density Φ and the scaling factor used in STAU can be found in Appendix D.

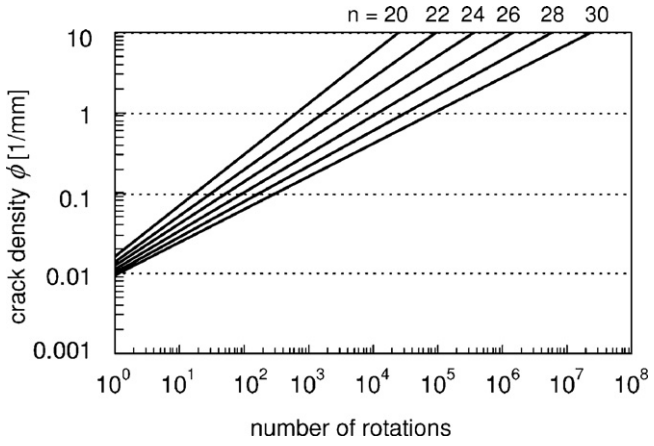

Fig. 10. Parametric study on crack density evolution: number of cycles needed to initiate a certain crack density on the roll surface with a probability of 63% for different values of the crack growth exponent n.

The following results were obtained for different scale factors corresponding to a certain crack density. The crack density which would be expected with a probability of 63% can be assigned to a number of cycles based on the characteristic lifetimes calculated. The results are shown in Fig. 10 for different crack growth exponents n. The extremely strong effect of n becomes obvious by comparing the number of rotations referring to $1\,mm^{-1}$. These differ by about two orders in magnitude within the selected range of n. Referring to the results in 4.3.2, the predicted crack density after 10^5 rotations exceeds $10\,mm^{-1}$ for n values below 22.

5. Discussion and conclusions

The scope of this study is to investigate the failure behaviour of ceramic components under sliding contact loading which is an important field of application for high strength ceramics. We have focused on probabilistic methods for modelling cyclic fatigue life of ceramics using the program STAU. A comprehensive study was conducted for a rolling contact fatigue test where time-dependent initiation of macroscopic cracks occurs on the ceramic friction partner. The prediction scheme is based on the idea that natural flaws act as initiation sites for numerous macroscopic cracks on the roll surface. Crack initiation is a local process and does not lead to catastrophic failure. In principle, this allows for studying the fatigue behaviour based on the time-dependent crack density observed in a single RCF test. Since the Weibull-theory is based on the idea that only one flaw becomes critical (weakest-link assumption), modelling the crack pattern generation for the entire roll has to be along a modified route. For that purpose, only a small section of the roll is modelled representing the un-cracked neighbourhood of a single crack. The failure probability then depends on the size of the modelled section which is inversely proportional to the corresponding crack density.

The time-dependent failure probability obtained for different fatigue parameters (Fig. 8) allows for a qualitative evaluation of the relevant failure mechanism. It is commonly accepted that predictions based on sub-critical crack growth lead to non-conservative predictions if cyclic fatigue with bridging degradation mechanisms is involved. On the other hand, cyclic crack propagation under the influence of water is promoted by SCG to a great extent, a fact which is reflected by the enhanced crack propagation rates (see Fig. 2(b)). This coincides with a study by Jacobs and Chen[22] showing that moist environments influence both the static and cyclic crack growth of Si_3N_4. It is therefore of utmost importance to consider the influence of environmental effects in the fatigue parameters especially if water-based lubricants are involved. Consequently, lifetimes based on the crack growth curve in water can be better compared with the damage observed in the RCF test.

The lack of a precise measurement of the crack density makes the assessment of prediction accuracy and a comparison with the experimental results difficult. The selected reference value of a crack density of $4\,mm^{-1}$ after 10 h (as obtained from Fig. 4(a)) can be regarded only as a rough estimate and should be considered mostly as a showcase example to study the influence of a variation in n and p on the crack growth curve in a water environment. However, it can be stated that a higher crack density than $4\,mm^{-1}$ can be expected after 10 h for lower values of n ($\Phi > 10\,mm^{-1}$ for $n < 22$). Furthermore, there is some uncertainty in n and p caused by the fact that only results for one load ratio were available in water ($R = 0.5$). Therefore, it was necessary to adopt p from the measurements in air, which were conducted for two different load ratios. This procedure implies that the relative shift between the crack growth curves (which is characterized by p) for $R = 0.1$ and $R = 0.5$ in air is the same as it would be in water. Results of the variation in p for typical p-values are presented in Fig. 9(b). The comparison to Fig. 9(a) shows that the uncertainty resulting from variations in p is quite small compared to the impact of n.

A major amount of uncertainty is associated with the systematic variation of n with the load ratio R. The crack growth relation (Eq. (3)) is inappropriate to account for any variation n. More elaborate crack growth laws as proposed e.g. by Fett and Munz[12] can account for this phenomenon but do not allow the backward integration (see also Eq. (5)) of the crack propagation which is necessary to calculate the failure probability. Therefore, we decided to consider the variation in n by means of a parametric study. As exponent in a power-law, n has a crucial effect on the failure probability and characteristic lifetimes obtained. It turns out that predictions agree better with the experiments for n set to somewhat smaller values of $n \approx 22$. These smaller values rather correspond to what is obtained for $R = 0.1$ (in air) which is close to $R = 0$ for the high stress region in the rolling contact (Fig. 7). Unfortunately, we do not have experimental data for $R = 0.1$ in water, but we argue that they may be reduced as well. This is justified by taking into account that the variation of n is due to a higher amount of wear damage at $R = 0.1$[18] and assuming that this mechanism is to some extent preserved under water.

Our probabilistic approach for the assessment of the reliability of rolling tools leads to some new insights in understanding their failure behaviour that may also be relevant for other high cycle fatigue loading cases. The fatigue and fracture behaviour of natural flaws becomes relevant if the maximum applied stresses in the vicinity of the contact are high enough to propagate small cracks. The partial cone cracks observed in the RCF test (Fig. 4) are characteristic for sliding contact loading. Finite element simulations conducted by Levesque and Arakere[23] support the conclusion that partial cone cracks can be originated from semi-elliptical surface cracks with a depth of about 10 μm. Such surface cracks are typically introduced by grinding with the crack shape being strongly dependent on the grinding direction (Quinn et al.[24]). In contrast, Lengauer and Danzer[1] stated that cracks below 50 μm are not critical for the failure of industrial rolls which exhibit maximum principal stresses of about 600 MPa in the calibre. In our work, however, the tensile stress magnitude in the RCF test is much higher and in the range of the inert strength of SL200 which explains why the appearance of several cracks is already seen and predicted immediately after the very first cycle (Fig. 10). Of course, fatigue crack propagation of cone cracks that have

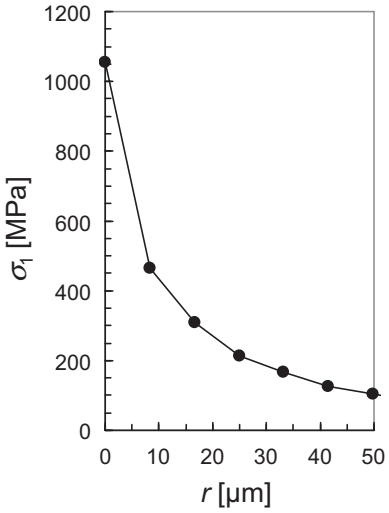

Fig. 11. Distribution of the maximum principal stress from FE-analysis along the direction of the roll depth.

initiated from natural flaws cannot be accounted for by our approach.

Some restrictions of the probabilistic approach with respect to the fracture mechanics and FE model employed should also be mentioned. First, our procedure implies that the crack density on the surface is limited to one crack per considered volume since the underlying FE-analysis refers to the un-cracked situation. Second, we use the normal stress criterion to determine the equivalent stress which means that only the Mode-I contribution is considered. Under contact loading, Mode-II contributions are important as well which can be seen from the fact that cracks kink at about 10 µm below the surface (Fig. 5). Accepting that Mode-I obviously governs the crack propagation in the vicinity of the surface, the normal stress criterion seems adequate for Si_3N_4 which exhibits comparably small natural cracks. It is also possible that slow crack growth occurs under the influence of Mode-II[25] when passing the compression zone. Unfortunately, measurements that could support this idea, such as cyclic tests at $R=-1$, are not available for SL200. Third, strong stress gradients occur under the roll surface. Fig. 11 shows that the tensile stress decreases by almost a factor of 2 within the first 10 µm. Such a strong gradient is not being considered, since stresses are assumed to be constant over the size of the flaws. For the case of spontaneous failure, a modified Weibull theory has been developed with an adequate fracture mechanics description for stress gradients,[26] but this procedure cannot be easily extended to cyclic crack propagation. Our predictions are therefore based on the maximum stresses at the surface, which is at least a conservative assumption.

6. Summary

The rolling contact fatigue test is a challenging example to study the usability of the probabilistic theory for ceramics with respect to fatigue effects. The probabilistic framework introduced in this work allows for predicting the crack density on the roll surface based on the idea that large (macroscopic) cracks are originated from natural flaws under cyclic loading. The developed simulation tool is validated in comparison to rolling experiments conducted for silicon nitride SL200 in water-based lubricants using independent input parameters obtained from fatigue experiments. It turns out that the presence of water is crucial for the prediction of the failure behaviour as the crack propagation is much faster than in a dry ambience. A parametric study of the fatigue lifetime shows that the prediction depends sensitively on the crack propagation parameters which may be a function of the loading ratio. We successfully demonstrated that a weakest-link approach, which considers besides spontaneous failure cyclic crack propagation from natural flaws, can be included to numerical tools based on FE simulations. As a result, the prediction of component reliability of lifetime becomes possible, which is an essential contribution for a reliable design of ceramic components in many technological applications.

Acknowledgements

The authors would like to thank Dr. Thomas Schwind for providing the fatigue data under water ambience and for the valuable discussions. Furthermore, the support of Gabriele Rizzi and Dr. Stefan Fünfschilling is highly appreciated.

The financial support by the "Deutsche Forschungsgemeinschaft" (German Research Foundation, DFG) is gratefully acknowledged. This work was performed within the framework of the Collaborative Research Centre 483 "High-performance sliding and friction systems based on advanced ceramics" at the Karlsruhe Institute of Technology (KIT).

Appendix A. Derivation of the failure probability

The failure probability of a component with exactly one flaw of arbitrary location and orientation reads (according to 26):

$$Q_1 = \frac{1}{V}\int_V \frac{1}{4\pi}\int_\Omega \left(\frac{\tilde{a}}{\min\limits_{N\in[0,N_k]}\left[a_{c,0}(N)\right]}\right)^{r-1} \mathrm{d}\Omega\,\mathrm{d}V \quad (A.1)$$

It is assumed that the probability to find a certain number of flaws in the component volume V is determined by a Poisson distribution with the parameter $M = (M_0/V_0)V$, in which M_0 is the mean number of flaws with respect to the unit volume V_0. The failure probability for an arbitrary number of flaws can be expressed as in Eq. (A.2):

$$P_f = 1-\exp(-MQ_1) = 1-\exp\left[\frac{M}{V}\int_V \frac{1}{4\pi}\int_\Omega \left(\frac{\tilde{a}}{\min\limits_{N\in[0,N_k]}\left[a_{c,0}(N)\right]}\right)^{r-1} \mathrm{d}\Omega\,\mathrm{d}V\right] \quad (A.2)$$

Eq. (9) follows from Eq. (A.2) by setting

$$m = 2(1-r) \qquad \sigma_0 = K_{Ic}(M_0^{1/m} Y_I \tilde{a}^{1/2})^{-1} \tag{A.3}$$

Appendix B. Cyclic crack growth for surface flaws

For surface flaws, the integral in Eq. (9) reads:

$$P_f = 1 - \exp\left(-\frac{1}{A_0}\int_A \frac{1}{2\pi}\int_\alpha I \,\mathrm{d}\alpha\,\mathrm{d}A\right). \tag{B.1}$$

where A is the component surface and α is the crack orientation based on the idea of a crack path perpendicular to the surface. The integrand reads the same as in Eqs. (9), (11) and (12). A_0 is a unit area. In this case, the integral must be solved over 3 dimensions: two spatial directions (A) and one orientation angle (α).

Appendix C. Sub-critical crack growth

The crack propagation rate $\mathrm{d}a/\mathrm{d}t$ can be described in terms of the applied stress intensity factor K_I by the power-law:

$$\frac{\mathrm{d}a}{\mathrm{d}t} = A_{sub}\left(\frac{K_I}{K_{Ic}}\right)^{n_{sub}}. \tag{C.1}$$

The parameters A_{sub} and n_{sub} are material properties. The failure probability (for volume flaws) reads (according to 9):

$$P_f = 1 - \exp\left(-\frac{1}{V_0}\int_V \frac{1}{4\pi}\int_\Omega \max_{t\in[0,t_0]} \left[\left(\frac{\sigma_{eq}(t)}{\sigma_0}\right)^{n_{sub}-2} + \frac{\sigma_0^2}{B}\int_0^t \left(\frac{\sigma_{eq}(\tau)}{\sigma_0}\right)^{n_{sub}}\mathrm{d}\tau\right]^{m/(n_{sub}-2)} \mathrm{d}\Omega\,\mathrm{d}V\right). \tag{C.2}$$

B is calculated from A_{sub} according to Eq. (10). An integral over the time-dependent load history $\sigma_{eq}(\tau)$ in the time interval of interest $t\in[0,t_0]$ is part of the integrand. The corresponding formulation for surface flaws is straightforward.

Appendix D. Crack density

A crack density analysis in STAU is possible by introducing a scaling factor k_{scale} in the calculation of N_0. The scaling factor is a multiple of the surface area A_{STAU} considered in the STAU calculation which, in our case, refers to the 500 μm section of the roll. k_{scale} must be chosen according to the surface area A_i, for which the failure probability or N_0 shall be determined:

$$k_{scale} = \frac{A_i}{A_{STAU}}. \tag{D.1}$$

Eq. (D.2) shows the characteristic lifetime (for surface flaws) under consideration of the scaling factor which refers to A_i based on the integration over the modelled section A_{STAU}:

$$N_0 = \left\{ 2k_{scale}\cdot\left[\frac{1}{A_0}\int_V \frac{1}{2\pi}\int_\alpha \left(\frac{\sigma_0^2}{B}\int_0^{N_k}\left(\frac{\sigma_{eq,max}(N)}{\sigma_0}\right)^n\cdot(1-R(N))^p\,\mathrm{d}N\right)^{m/(n-2)}\mathrm{d}\alpha\,\mathrm{d}A\right]\right\}^{-1/m^*} \tag{D.2}$$

The factor 2 which precedes k_{scale} in Eq. (D.2) is specific for the present analysis and accounts for the fact, that we only modelled half of the roll for symmetry reasons. N_0 refers to the number of rotations required to initiate one single crack in the considered section A_i with a probability of 63%. The total number of cracks on the roll n_{tot} is thus given by the ratio of the total roll surface A_{tot} and the considered area A_i:

$$n_{tot} = \frac{A_{tot}}{A_i} = \frac{A_{tot}}{k_{scale}A_{STAU}}. \tag{D.3}$$

Eq. (D.3) relates the scaling factor and the specific area considered in STAU to the total number of cracks on the roll, n_{tot}. From geometrical considerations, n_{tot} can be related to the crack density Φ defined as total number of cracks along the roll circumference:

$$\phi = \frac{n_{tot}}{\pi d_{roll}}. \tag{D.4}$$

The relation between crack density Φ and scaling factor k_{scale} follows by inserting Eq. (D.4) into Eq. (D.3):

$$k_{scale} = \frac{1}{\phi\pi d_{roll}}\cdot\frac{A_{tot}}{A_{STAU}}. \tag{D.5}$$

For the cylindrical roll under consideration, the ratio of the outer surface areas A_{tot}/A_{STAU} is proportional to the ratio of the corresponding circumference section lengths c_{tot} and c_{STAU}: $(A_{tot}/A_{STAU}) \propto (c_{tot}/c_{STAU}) = (\pi d_{roll}/c_{STAU})$. Consequently, Eq. (D.5) reduces to:

$$k_{scale} = \frac{1}{\phi\cdot c_{STAU}}. \tag{D.6}$$

In our case, the circumference section length $c_{STAU} = 500\,\mu m$ is the roll section which was modelled in the FE analysis. Consequently, predicting the characteristic lifetime N_0 which refers to initiating a crack density of $\phi = 1/500\,\mu m^{-1}$ ($n_{tot}\approx 346$) requires a scaling factor of $k_{scale} = 1$ (Eq. (D.6)). If N_0 shall refer to having one single crack along the total roll circumference ($\phi = 1/\pi d_{roll} = 1/(\pi\cdot 55)\,mm^{-1}$, $n_{tot} = 1$), the scaling factor must be set $k_{scale}\approx 346$.

References

1. Lengauer M, Danzer R. Silicon nitride tools for the hot rolling of high-alloyed steel and superalloy wires – crack growth and lifetime prediction. *Journal of the European Ceramic Society* 2008;**28**:2289–98.

2. Danzer R, Lengauer M. Silicon nitride materials for hot working of high strength metal wires. *Engineering Failure Analysis* 2010;**17**:596–606.
3. Khader I, Kailer A. Damage mechanisms in silicon nitride wire-rolling tools: lab-scale experiments and correlation with finite element modeling. *Journal of Materials Processing Technology* 2010;**210**:1314–25.
4. Weibull W. *A statistical theory of the strength of materials*. Stockholm: Generalstabens Litografiska Anstalts Förlag; 1939.
5. Riesch-Oppermann H, Härtelt M, Kraft O. Stau – a review of the Karlsruhe weakest link finite element postprocessor with extensive capabilities. *International Journal of Materials Research* 2008;**99**:1055–65.
6. Nemeth N, Jadaan O, Gyekenyesi J. Lifetime reliability prediction of ceramic structures under transient thermomechanical loads. *Technical report*, NASA/TP-2005-212505; 2005.
7. Wiederhorn SM. Moisture assisted crack growth in ceramics. *International Journal of Fracture* 1968;**4**:171–7.
8. Dauskardt R. A frictional-wear mechanism for fatigue-crack growth in grain bridging ceramics. *Acta Metallurgica et Materialia* 1993;**41**:2765–81.
9. Brückner-Foit A, Ziegler C. Design reliability and lifetime prediction of ceramics. In: Vincenzini P, editor. *Cermics: getting into the 2000's. Proceedings of the world ceramics congress*. 1999. p. 585–95.
10. Batdorf SB, Heinisch HL. Weakest link theory reformulated for arbitrary fracture criterion. *Journal of the American Ceramic Society* 1978;**61**:355–8.
11. Brückner-Foit A, Fett T, Munz D, Schirmer K. Discrimination of multiaxiality criteria with the brazilian disc test. *Journal of the European Ceramic Society* 1997;**17**:689–96.
12. Fett T, Munz D. A relation for cyclic crack growth in ceramics. *Journal of Materials Science Letters* 1998;**17**:307–9.
13. Munz D, Fett T. *Ceramics, mechanical properties, failure behaviour, materials selection*. Berlin/Heidelberg: Springer Verlag; 1999.
14. *DIN EN 843-1, Hochleistungskeramik – Mechanische Eigenschaft monolithischer Keramik bei Raumtemperatur – Teil 1: Bestimmung der Biegefestigkeit*. Berlin: Beuth Verlag; 2008.
15. Schwind T, Schalk T, Kerscher E, Beck T, Lang K, Löhe D. Thermal, mechanical and fretting fatigue of silicon nitride. *International Journal of Materials Research* 2008;**99**:1090–7.
16. Lube T, Dusza J. A silicon nitride reference material – a testing program of ESIS TC6. *Journal of the European Ceramic Society* 2007;**27**:1203–9.
17. Fett T, Martin G, Munz D, Thun G. Determination of da/dN-ΔK_1 curves for small cracks in alumina in alternating bending tests. *Journal of Materials Science* 1991;**26**:3320–8.
18. S. Fünfschilling, Mikrostrukturelle Einflüsse auf das R-Kurvenverhalten bei Siliciumnitridkeramiken. PhD Thesis. Karlsruhe: KIT Scientific Publishing; 2010. ISBN: 9783866444706.
19. T. Schwind, Untersuchung zum zyklischen Ermüdungsverhalten von Si3N4 und Al2O3 ausgehend von natürlichen Fehlern. PhD thesis. Karlsruhe Institute of Technology. 065, Shaker Verlag, Aachen; 2010. ISBN: 978-3-8322-9691-9.
20. Khader I. Damage mechanisms in silicon nitride rolling tools applied in caliber rolling copper and steel wires. PhD thesis. Karlsruhe Institute of Technology. 062. Aachen: Shaker Verlag; 2010. ISBN: 978-3-8322-9389-5.
21. Lawn B. Partial cone crack formation in a brittle material loaded with a sliding spherical indenter. *Proceedings of the Royal Society of London, Series A* 1967;**299**:307–16.
22. Jacobs DS, Chen IW. Mechanical and environmental factors in the cyclic and static fatigue of silicon nitride. *Journal of the American Ceramic Society* 1994;**77**:1153–61.
23. Levesque G, Arakere NK. An investigation of partial cone cracks in silicon nitride balls. *International Journal of Solids and Structures* 2008;**45**:6301–15.
24. Quinn GD, Ives LK, Jahanmir S. Machining cracks in finished ceramics. *Key Engineering Materials* 2005;**290**:1–13.
25. Fett T. Interpretation of failure under cyclic contact loading. *Journal of Materials Science* 2004;**39**:1795–7.
26. Licht V, Hülsmeier P, Fett T. Probability of cone crack initiation due to spherical contact loading. *Journal of the European Ceramic Society* 2004;**24**:2907–15.